DOI 10.1007/s11106-017-9889-1
Powder Metallurgy and Metal Ceramics, Vol. 56, Nos. 3-4, July, 2017 (Russian Original Vol. 56, Nos. 3-4, March-April, 2017)

PHASE EQUILIBRIA IN THE Cu–Ti–Zr SYSTEM AT 750°C. II. THE ISOTHERMAL SECTION WITH COPPER CONTENT FROM 50 TO 100 at.%

A. M. Storchak-Fedyuk,[1,4] L. V. Artyukh,[1] A. V. Grytsiv,[2] P. G. Agraval,[3] M. A. Turchanin,[3] and T. Ya. Velikanova[1]

UDC 669.017

Alloys of the ternary Cu–Ti–Zr system with 50–100 at.% Cu, annealed at 750°C, are studied by scanning electron microscopy, electron microprobe analysis, and X-ray diffraction. The isothermal section at 750°C is constructed in this composition range. A new hexagonal ternary phase of composition $Cu_{63.5}Ti_{14.5}Zr_{22}$ is found.

Keywords: *Cu–Ti–Zr system, microstructure, isothermal section.*

INTRODUCTION

The first paper [1] of the series provides a brief overview of the literature on phase equilibria in the ternary Cu–Ti–Zr system [2–8] and presents our own experimental results as the isothermal section of the phase diagram at 750°C with copper content from 0 to 50 at.% [1]. It is shown that the τ_1 ternary phase (Laves phase of $MgZn_2$ type) has an appreciable homogeneity range at 750°C. Its extension by copper is ~7 at.% (in a range from 42.6 to 49.8 at.% Cu) and by titanium is about 8 at.% (in a range from 20 to 28 at.% Ti). The copper content of the β-(Ti, Zr) bcc solid solution at 750°C becomes higher when Ti content increases from 1.5 at.% (at 11 at.% Ti) to ~4 at.% (at 81.5 at.% Ti). The continuous series of solid solutions [$Cu(Ti, Zr)_2$, $MoSi_2$ type], i.e., the γ phase, is linear by copper content (within the error of electron microprobe analysis). To construct the section, the boundary binary Cu–Ti [9], Cu–Zr, and Ti–Zr phase diagrams were used [10]. The data obtained on the constant (CuX_2) copper content of the γ phase support the Cu–Ti phase diagram according to which $CuTi_2$ compound has no homogeneity range [9].

Our objective is to study the Cu–Ti–Zr system at 750°C in the range 50–100 at.% Cu. Additional study of the system is necessitated by distinctions in the phase equilibria not only at different temperatures (703°C [5] or 750°C [6]), but also at the same temperature, 800°C, in [7, 8]. Table 1 briefly outlines the analysis methods and composition–temperature ranges of the phase diagram according to different researchers. Special attention is paid to the purity of starting materials and alloy production conditions (synthesis and heat treatment of the samples) since they can substantially influence the alloy structure and, accordingly, phase equilibria.

The crystallographic data on interim binary and ternary phases of the Cu–Ti–Zr system at copper content from 50 to 100 at.% are provided in Table 2.

[1]Frantsevich Institute for Problems of Materials Science, National Academy of Sciences of Ukraine, Kiev, Ukraine. [2]Institute of Physical Chemistry, University of Vienna, Austria. [3]Donbass State Mechanical Engineering Academy, Kramatorsk, Ukraine.

[4]To whom correspondence should be addressed; e-mail: asyasf@bigmir.net.

Translated from Poroshkovaya Metallurgiya, Vol. 56, Nos. 3–4 (514), pp. 131–142, 2017. Original article submitted July 8, 2016.

TABLE 1. Phase Equilibria in the Cu–Ti–Zr System According to Different Published Data

Ref.	Starting materials	Production method; annealing time	Analysis methods	Composition range for analysis of the phase diagram
[2]	OFHC copper, *Bureau of Mines* electrolytic titanium (Bhn 63), reactor-grade zirconium (Bhn <150)	Arc melting; homogenizing annealing 825°C/48 h, 750°C/5 days, quenched in ice brine with capsule breaking	OM, XRD, annealed samples	Titanium corner <50 wt.% Ti at 750°C
[3]	Electrolytic copper (99.99%), iodide-refined titanium and zirconium (99.98%)	Arc melting; 970°C/200 h, water-cooled capsules	OM, XRD, DTA, HV	Vertical section $CuTi_2$–$CuZr_2$
[4]	Electrolytic copper (99.99%), iodide-refined titanium and zirconium (99.98%)	Arc melting; 700°C/200 h	OM, XRD, DTA	Vertical section CuTi–CuZr
[5]	Copper (99.999%), titanium (99.98%), and zirconium (99.95%) of high purity	Arc melting; 703°C/14 days, quenched with capsule breaking	OM, EMPA, diffusion couple method with reactive liquid phase	$x > 0.3$, isothermal section at 703°C, liquidus in central part of phase diagram
[6]	Copper (99.99%), titanium (99.99%), and zirconium (99.9%)	Diffusion triples obtained at 750°C; 750°C/1404 h, quenched	Diffusion triple method, SEM, EMPA	Isothermal section at 750°C
[1]	Electrolytic copper (99.99 wt.%), iodide-refined titanium (99.94 wt.%) and zirconium (99.96 wt.%)	Arc melting; 750°C/536 h, quenched	OM, SEM, EMPA, XRD	Partial isothermal section at 750°C in range 0–50 at.% Cu
[7]	Titanium (99.98%) and zirconium (99.9%), copper (99.999%), supplied by Alfa Aesar, Jonson Matthey & Brandenberger, Zurich, Switzerland	Arc melting; alloys: 800°C/ 760 h, brine quenched. Cut diffusion couples: 800°C/264 h	Diffusion couple method, annealed alloys, OM, SEM, EMPA, differential scanning calorimetry	Isothermal section at 800°C
[8]	Titanium (99.98%) and zirconium (99.0%), copper (99.9%), supplied by Alfa Aesar	Arc melting; 800°C/14 days, water quenched	OM, SEM, EMPA, XRD	Isothermal section at 800°C

Note. OM—optical (light microscopy); XRD—X-ray diffraction; DTA—differential thermal analysis; HV—microhardness; EMPA—electron microprobe analysis; SEM—scanning electron microscopy.

EXPERIMENTAL PROCEDURE

Ternary alloys of more than 20 compositions (Table 3, Fig. 1) were melted for the experimental study in this region. The starting materials were electrolytic copper (99.99 wt.%) and iodide-refined titanium (99.94 wt.%) and zirconium (99.96 wt.%). The ingots with a weight of 10 g were melted in an arc furnace with a nonconsumable tungsten electrode on a water-cooled copper hearth in an argon atmosphere purified by melting titanium–zirconium getter (argon pressure ~80 kPa) for 5 min. The ingots were cooled down at a rate of ~100°C/sec.

The ingots were flipped and remelted at least three times to avoid inhomogeneity of chemical composition. Since the weight loss after melting was no more than 0.2 wt.%, the alloy composition was accepted as in the starting charge. The presence of admixtures in the starting copper and, selectively, in the annealed alloys was checked with spectral (ternary alloys $Cu_{55}Ti_{25}Zr_{20}$ (sample 32), $Cu_{63.5}Ti_{14.5}Zr_{22}$ (sample 36), and $Cu_{63.5}Ti_{20}Zr_{16.5}$ (sample 37)) and chemical (binary alloys $Cu_{27.6}Zr_{72.4}$ and $Cu_{33.3}Zr_{66.7}$) analyses. It is shown that the ternary alloys contain 10^{-2}–10^{-3} wt.% and less of Fe admixtures, 10^{-1}–10^{-2} wt.% and less of Ni, and 10^{-1} wt.% Zn; Al, Mo, Si, and W were not revealed. The oxygen content of binary alloys $Cu_{27.6}Zr_{72.4}$ and $Cu_{33.3}Zr_{66.7}$ is 0.052 and 0.014 wt.%, respectively, while N and H were not revealed.

TABLE 2. Crystallographic Data of the Phases Existing in the Cu–Ti–Zr System at 50–100 at.% Cu

Phases; temperature range of stability, °C	Pearson symbol; space group; prototype	Lattice parameters, pm	Comment, reference
(Cu); <1084.87	*cF*4; $Fm\bar{3}m$; Cu	*a* = 361.46	Cu at 25°C [10]
Cu_5Zr; <1012	*cF*24; $F\overline{43}m$; $AuBe_5$	*a* = 687.0	[10, 11]
$Cu_{51}Zr_{14}$; <1115	*hP*68; *P*6/*m*; $Gd_{14}Ag_{51}$	*a* = 1124.44 *c* = 828.15	[10, 11]
Cu_8Zr_3; <975	*oP*44; *Pnma*; Hf_3Cu_8	*a* = 786.93 *b* = 815.47 *c* = 998.48	[10, 11]
$Cu_{10}Zr_7$; <895	*oC*68; *C*2*ca*; Zr_7Ni_{10}	*a* = 1267.29 *b* = 931.63 *c* = 934.66	[11, 10]
CuZr; 935–715	*cP*2; $Pm\bar{3}m$; CsCl	*a* = 326.0	[10, 11]
βCu_4Ti; 885…~400	*oP*20; *Pnma*; $ZrAu_2$	*a* = 452.5 *b* = 434.1 *c* = 1295.1	~78.6…~80.9 at.% Cu [9]
αCu_4Ti; <500	*tI*10; *I*4/*m*; $MoNi_4$		~78.6…~80.9 at.% Cu [9]
Cu_2Ti; 890–870	*oC*12; *Amm*2; Au_2V	*a* = 436.3 *b* = 797.7 *c* = 447.8	[9]
Cu_3Ti_2; <875	*tP*10; *P*4/*nmm*; Ti_2Cu_3	*a* = 313.0 *c* = 1395.0	[10, 11]
Cu_4Ti_3; <925	*tI*14; *I*4/*mmm*; Ti_3Cu_4	*a* = 313.0 *c* = 1994.0	[10, 11]
CuTi; <982	*tP*4; *P*4/*nmm*; CuTi	*a* = 312.5 *c* = 591.5	[10, 11]
τ_1, Cu_2TiZr; <867	*hP*12; $P6\bar{3}/mmc$; $MgZn_2$	*a* = 513.0 *c* = 825.0	[12] (ternary phase composition is mistakenly indicated as Cu_4TiZr) 25 at.% Zr, 25 at.% Ti, 50 at.% Cu at 867°C; 21–37 at.% Zr with 50 at.% Cu at ~830°C; 22.5–29 at.% Zr with 50 at.% Cu at ~630°C [4]; from 25 to 30 at.% Zr with 45 to 50 at.% Cu at 703°C [5]
859.7			25 at.% Zr, 25 at.% Ti, 50 at.% Cu [7]
τ_2	Hexagonal	*a* = 514.91 *c* = 824.21	[13]

The alloy samples (from 6 to 13 pieces), each being wrapped in titanium foil, were placed in a quartz capsule 25 mm in diameter and 170 mm in length, considering extension of the hot area (100–110 mm). The capsule walls and lower and upper parts were additionally insulated with titanium foil and shavings. Then the capsule was evacuated and filled with argon (excess pressure ~30,397 Pa). Three to six capsules were placed into a ceramic crucible. The space between the capsules, as well as between the capsules and crucible wall, was filled with sand to decrease temperature gradient in the furnace during annealing. The samples, except for alloys $Cu_{53}Ti_{11}Zr_{36}$ (sample 30), $Cu_{63.5}Ti_{14.5}Zr_{22}$ (sample 36), $Cu_{63.5}Ti_{20}Zr_{16.5}$ (sample 37), $Cu_{63.5}Ti_{29.5}Zr_7$ (sample 38), and $Cu_{70}Ti_2Zr_{28}$ (sample 39), were annealed in an electric muffle furnace at 750°C for 536 h. Alloys 30 and 36–39 were annealed in two steps—200 h and 523 h at the same temperature. Following annealing, the capsules with the samples were placed into cold water without breaking because of high activity of the metal components.

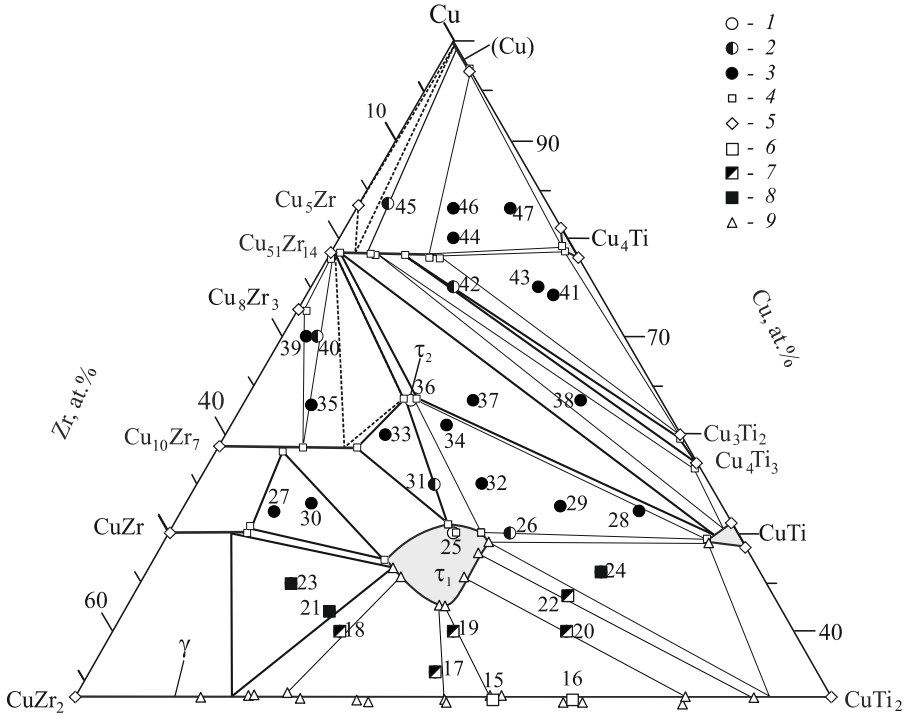

Fig. 1. Isothermal section at 750°C of the ternary Cu–Ti–Zr system in the $CuTi_2$–Cu–$CuZr_2$ region: single-phase (*1*), two-phase (*2*), and three-phase (*3*) alloys; EMPA data (*4*); published data [9, 10] (*5*); single-phase (*6*), two-phase (*7*), and three-phase (*8*) alloys [1]; EMPA data [1] (*9*)

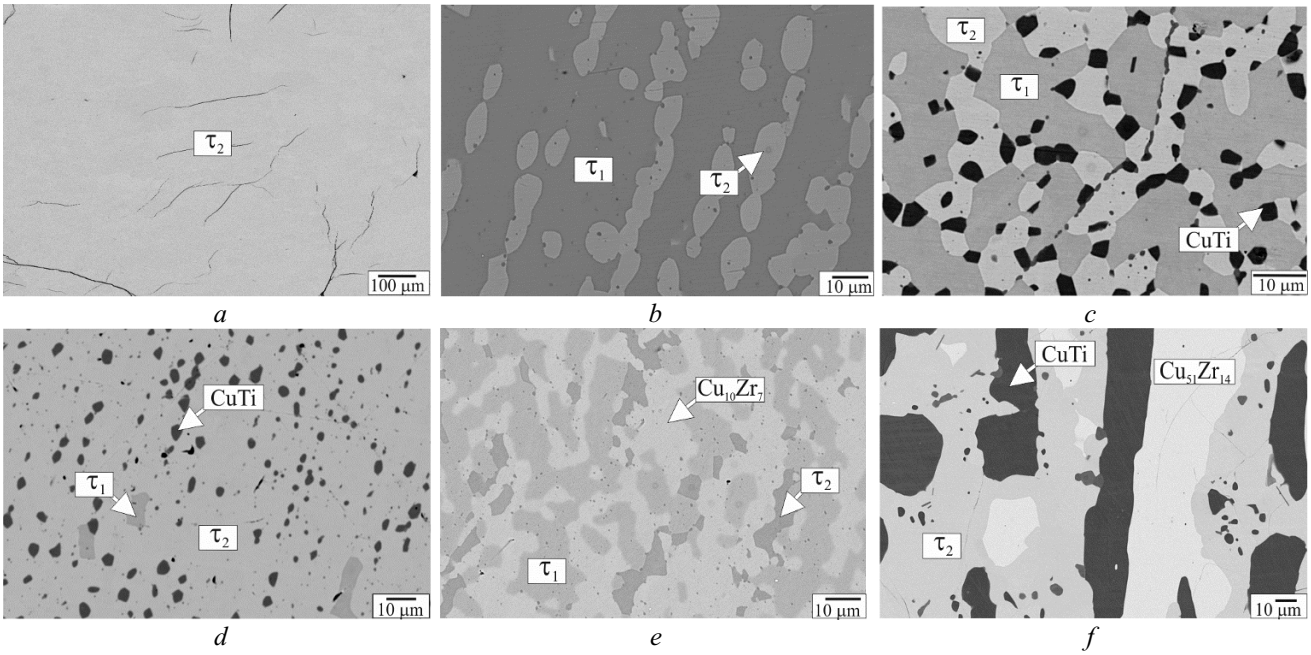

Fig. 2. Microstructure (in backscattered electrons) of alloys 36 (*a*), 31 (*b*), 32 (*c*), 34 (*d*), 33 (*e*), 37 (*f*) containing the τ_2 phase in the Cu–Ti–Zr system

The alloys were examined by XRD, OM, SEM, and EMPA. The alloy microstructures are represented by well-faceted phase grains with clear boundaries. This indicates that the annealing time was sufficient to reach the equilibrium state. The X-ray diffraction patterns were taken with a DRON-3 diffractometer for powders or sections in filtered copper radiation (Cu-K_α, $\lambda = 0.1542$ nm) and processed using the PowderCell 2.2 full-profile analysis software.

TABLE 3. Phase Composition of the Cu–Ti–Zr Alloys Annealed at 750°C According to SEM, XRD, and EMPA

Alloy No.*	Alloy, at.%	Alloy phase constituents	Phase	Phase composition, at.%		
				Cu	Ti	Zr
25	$Cu_{50}Ti_{25}Zr_{25}$	τ_1	τ_1	50.0	25.2	24.8
26	$Cu_{50}Ti_{30}Zr_{20}$	τ_1 + (CuTi)**	τ_1	49.8	27.5	22.7
			(CuTi)	49.1	47.7	3.2
27	$Cu_{52.3}Ti_{7.8}Zr_{39.9}$	(CuZr) + ($Cu_{10}Zr_7$) + τ_1	(CuZr)	49.2	7.3	43.5
			($Cu_{10}Zr_7$)	58.6	5.7	35.7
			τ_1	47.4	20.1	32.5
28	$Cu_{52.3}Ti_{40}Zr_{7.7}$	τ_1 + τ_2 + (CuTi)	τ_1	50.4	27.2	22.4
			τ_2	63.7	15.1	21.2
			(CuTi)	49.3	48.0	2.7
29	$Cu_{52.7}Ti_{33.1}Zr_{14.2}$	τ_1 + τ_2 + (CuTi)	τ_1	50.1	27.4	22.5
			τ_2	63.6	14.9	21.5
			(CuTi)	49.3	47.3	3.4
30	$Cu_{53}Ti_{11}Zr_{36}$	(CuZr) + ($Cu_{10}Zr_7$) + τ_1	(CuZr)	48.8	7.2	44.0
			($Cu_{10}Zr_7$)	57.4	5.9	36.7
			τ_1	46.9	20.5	32.6
31	$Cu_{55}Ti_{20.7}Zr_{24.3}$	τ_1 + τ_2	τ_1	50.8	24.1	25.1
			τ_2	62.8	14.5	22.7
32	$Cu_{55}Ti_{25}Zr_{20}$	τ_1 + τ_2 + (CuTi)	τ_1	49.5	27.4	23.1
			τ_2	63.5	14.7	21.8
			(CuTi)	48.9	47.6	2.6
33	$Cu_{60}Ti_{14}Zr_{26}$	τ_1 + τ_2 + ($Cu_{10}Zr_7$)	τ_1	50.8	24.1	25.1
			τ_2	63.6	13.8	22.6
			($Cu_{10}Zr_7$)	58.6	12.2	29.2
34	$Cu_{61}Ti_{19}Zr_{20}$	τ_2 + (CuTi) + τ_1	τ_2	64	14.7	21.3
			CuTi	50.1	47.1	2.8
			τ_1	50.5	27.4	22.1
35	$Cu_{63}Ti_6Zr_{31}$	($Cu_{10}Zr_7$) + (Cu_8Zr_3) + ($Cu_{51}Zr_{14}$)	($Cu_{10}Zr_7$)	59.4	7.6	33.0
			(Cu_8Zr_3)	72.0	1.6	26.4
			($Cu_{51}Zr_{14}$)	77.8	0.4	21.8
36	$Cu_{63.5}Ti_{14.5}Zr_{22}$	τ_2	τ_2	63.2	14.2	22.6
37	$Cu_{63.5}Ti_{20}Zr_{16.5}$	($Cu_{51}Zr_{14}$) + τ_2 + (CuTi)	($Cu_{51}Zr_{14}$)	77.4	1.1	21.5
			τ_2	63.2	14.9	21.9
			(CuTi)	48.7	48.6	2.7
38	$Cu_{63.5}Ti_{29.5}Zr_7$	($Cu_{51}Zr_{14}$) + (Cu_4Ti_3) + (CuTi)	($Cu_{51}Zr_{14}$)	76.7	4.9	18.4
			(Cu_4Ti_3)	56.4	43.0	0.6
			(CuTi)	50.0	49.6	0.4
39	$Cu_{70}Ti_2Zr_{28}$	($Cu_{10}Zr_7$) + (Cu_8Zr_3) + ($Cu_{51}Zr_{14}$)	($Cu_{10}Zr_7$)	58.4	5.5	36.1
			(Cu_8Zr_3)	71.6	1.1	27.3
			($Cu_{51}Zr_{14}$)	77.7	0.2	22.1
40	$Cu_{70}Ti_3Zr_{27}$	($Cu_{51}Zr_{14}$) + ($Cu_{10}Zr_7$)	($Cu_{51}Zr_{14}$)	77.8	0.4	21.8
			($Cu_{10}Zr_7$)	58.5	6.8	34.7

Table 3 finished

Alloy No.*	Alloy, at.%	Alloy phase constituents	Phase	Phase composition, at.%		
				Cu	Ti	Zr
41	$Cu_{74.2}Ti_{21.1}Zr_{4.1}$	$(Cu_{51}Zr_{14}) + (Cu_4Ti) + (Cu_3Ti_2)$	$(Cu_{51}Zr_{14})$	N.d.***	N.d.	N.d.
			(Cu_4Ti)	N.d.	N.d.	N.d.
			(Cu_3Ti_2)	N.d.	N.d.	N.d.
42	$Cu_{75}Ti_{12.5}Zr_{12.5}$	$(Cu_{51}Zr_{14}) + (Cu_4Ti_3)$	$(Cu_{51}Zr_{14})$	77.8	7.3	14.9
			(Cu_4Ti_3)	56.5	43.2	0.3
43	$Cu_{75}Ti_{20}Zr_5$	$(Cu_{51}Zr_{14}) + (Cu_4Ti) + (Cu_3Ti_2)$	$(Cu_{51}Zr_{14})$	77.5	10.0	12.5
			(Cu_4Ti)	78.6	20.5	0.9
			(Cu_3Ti_2)	59.8	40.0	0.2
44	$Cu_{80}Ti_{10}Zr_{10}$	$(Cu_{51}Zr_{14}) + (Cu_4Ti) + (Cu)$	$(Cu_{51}Zr_{14})$	77.9	8.6	13.5
			(Cu_4Ti)	78.6	20.4	1.0
			(Cu)	N.d.	N.d.	N.d.
45	$Cu_{83}Ti_3Zr_{14}$	$(Cu_{51}Zr_{14}) + (Cu)$	$(Cu_{51}Zr_{14})$	77.9	8.3	13.8
			(Cu)	N.d.	N.d.	N.d.
46	$Cu_{83}Ti_{8.5}Zr_{8.5}$	$(Cu_4Ti) + (Cu_{51}Zr_{14}) + (Cu)$	$(Cu_{51}Zr_{14})$	78.6	8.5	12.9
			(Cu_4Ti)	79.4	19.7	0.9
			(Cu)	N.d.	N.d.	N.d.
47	$Cu_{83}Ti_{13.5}Zr_{3.5}$	$(Cu_4Ti) + (Cu_{51}Zr_{14}) + (Cu)$	$(Cu_{51}Zr_{14})$	78.1	9.0	12.9
			(Cu_4Ti)	79.3	19.6	0.9
			(Cu)	96.7	3.3	0

* Numbering begins in [1]. ** Compound-based solid solution is in parenthesis. *** N.d.—not determined.

TABLE 4. Angular Positions and Intensities of τ_2 Phase Reflections (2θ) in Alloy $Cu_{63.5}Ti_{14.5}Zr_{22}$ (Sample 36)

2θ, deg	Intensity, r.u.	Intensity, %	2θ, deg	Intensity, r.u.	Intensity, %
14.565	13530	23.58	50.965	6206	10.81
23.625	6931	12.08	56.555	6791	11.83
28.915	6169	10.75	61.430	5471	9.53
29.510	5240	9.13	62.280	8853	15.43
30.995	16089	28.04	62.675	7352	12.81
34.755	5602	9.76	64.750	5780	10.07
35.895	13236	23.07	65.290	5874	10.24
37.555	20328	35.42	67.335	4735	8.25
38.565	54154	94.37	67.655	5169	9.01
38.965	52122	90.83	69.190	8470	14.76
39.420	57384	100	70.405	6491	11.31
40.530	26727	46.58	73.305	7170	12.49
41.205	11053	19.26	74.385	10310	17.97
41.850	47567	82.89	74.980	15868	27.65
43.320	53642	93.48	76.250	6995	12.19
45.015	9652	16.82	77.165	6360	11.08
46.850	27886	48.60	78.235	9163	15.97
47.195	15892	27.69	80.720	4612	8.04
48.580	14657	25.54	82.675	5585	9.73
49.670	14145	24.65	85.810	5321	9.27

In addition, sample 36 was studied in a Guinier camera in monochromatic copper radiation (λ = = 0.154051 nm). Scanning electron microscopy and EMPA were carried out employing Superprobe JXA-8200 (JEOL Ltd., Japan), INCA Penta FETx3 (Oxford Instrument, United Kingdom), and Zeiss SUPRA55VP (Carl Zeiss Group, Germany).

RESULTS AND DISCUSSION

The chemical and phase compositions of the alloys annealed at 750°C are provided in Table 3. An isothermal section has been constructed in the $CuZr_2$–Cu–$CuTi_2$ region (Fig. 1).

In the alloys with 52.7 to 63.5 at.% Cu (Table 3), a new ternary phase was revealed (τ_2); its composition was determined as $Cu_{63.5}Ti_{14.5}Zr_{22}$ according to averaged EMPA data for alloys in adjacent phase regions. The alloy of the same composition that was produced additionally (sample 36) turned out to be single-phase after annealing at 750°C for 200 + 523 h (Fig. 2*a*), thus confirming the existence of the ternary compound. The homogeneity range of the new phase is not extensive and lies within the measurement error. The diffraction pattern of annealed alloy $Cu_{63.5}Ti_{14.5}Zr_{22}$ was taken in a Guinier camera in the range 0–100° at increment 2θ = 0.005° (Fig. 3*a*). Table 4 shows angular positions and intensities of the strongest reflections (2θ).

Comparison of the X-ray diffraction pattern for the new τ_2 phase (Fig. 3*a*) and theoretical diffraction patterns for the known ternary Laves phase, Cu_2TiZr (τ_1), and binary orthorhombic $Cu_{10}Zr_7$ and hexagonal $Cu_{51}Zr_{14}$

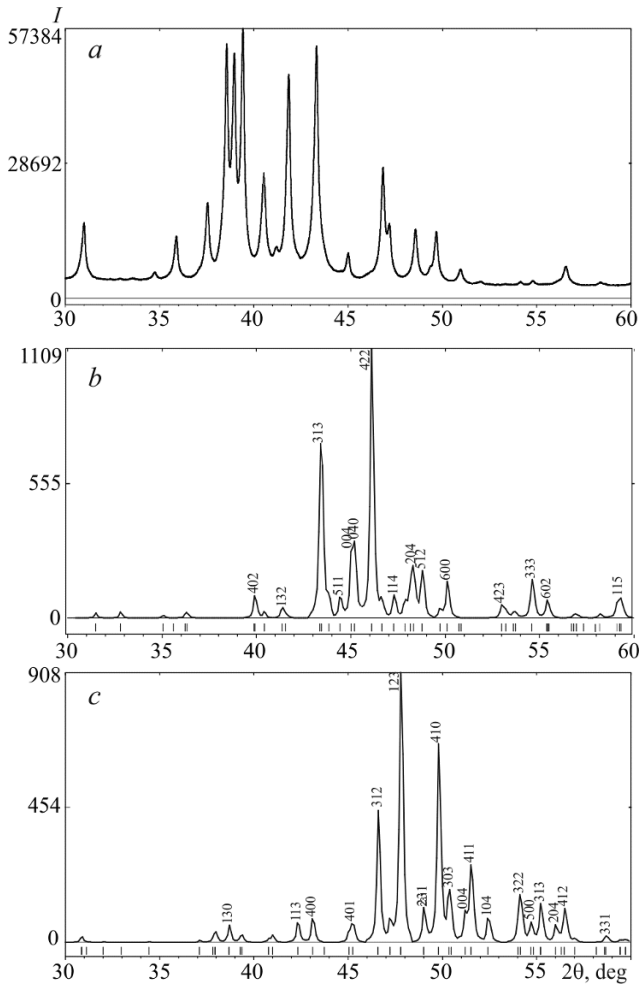

Fig. 3. X-ray diffraction patterns for phases of the ternary Cu–Ti–Zr system: *a*) experimental diffraction pattern for alloy 36; *b*, *c*) theoretical diffraction patterns for the $Cu_{10}Zr_7$ and $Cu_{51}Zr_{14}$ phases, respectively (indices are provided for the most intensive lines)

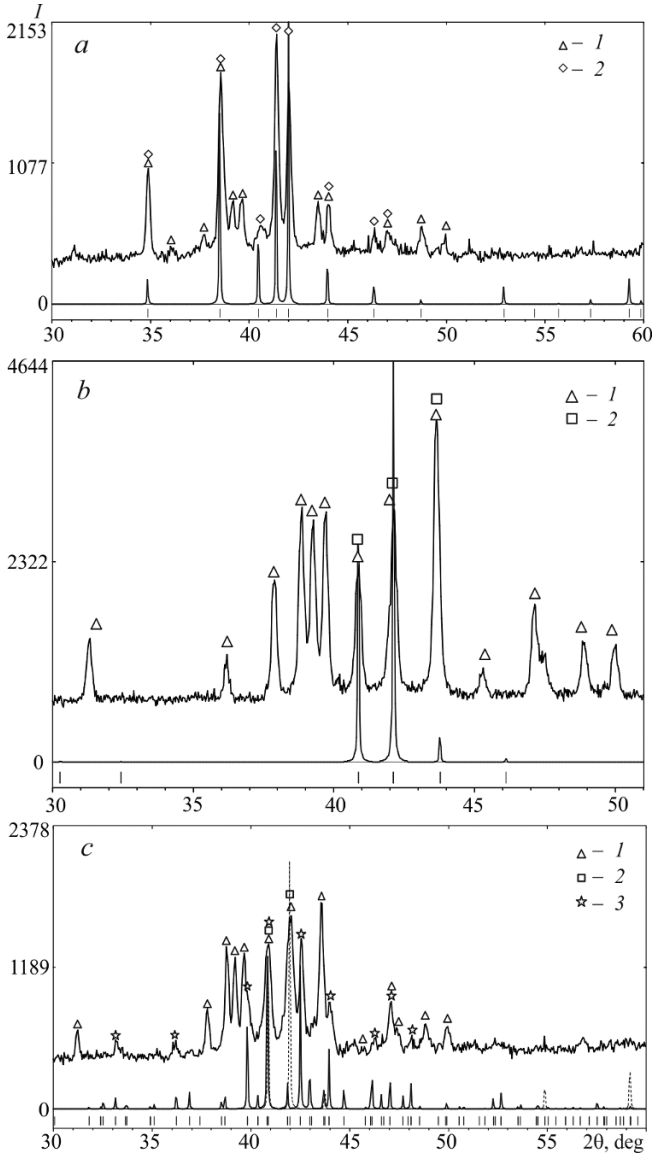

Fig. 4. Phase analysis of experimental X-ray diffraction spectra of the alloys: 31 (*a*), *1*—reflections of the τ_2 phase, *2*—reflections of the τ_1 phase; 34 (*b*), *1*—reflections of the τ_2 phase, *2*—reflections of the CuTi phase; 37 (*c*), *1*—reflections of the τ_2 phase, *2*—reflections of the CuTi phase, *3*—reflections of the $Cu_{51}Zr_{14}$ phase

compounds (Fig. 3*b*, *c*), which have extensive homogeneity ranges and coexist with the τ_2 phase at 750°C in the ternary system (Fig. 1), shows that they substantially differ in angular positions and intensity of reflections.

Hence, the crystal structure of the τ_2 phase is not identical to these compounds. We did not manage to obtain an isolated single crystal for crystallographic analysis. According to study of eight fragments of the annealed sample, the τ_2 phase has a 1200 pm × 980 pm hexagonal cell.

The microstructure of two-phase alloy $Cu_{55}Ti_{20.7}Zr_{24.3}$ (sample 31), which has two ternary phases ($\tau_1 + \tau_2$) according to EMPA and XRD, is shown in Fig. 2*b* and a fragment of its experimental diffraction pattern in Fig. 4*a*. These ternary compounds have very close microhardness, differing within the measurement error and constituting ~6.0 GPa. These two phases also differ only little in contrast in backscattered electrons. Therefore, only EMPA can be used for reliable identification (and differentiation) of these ternary compounds in metallographic analysis of the alloys.

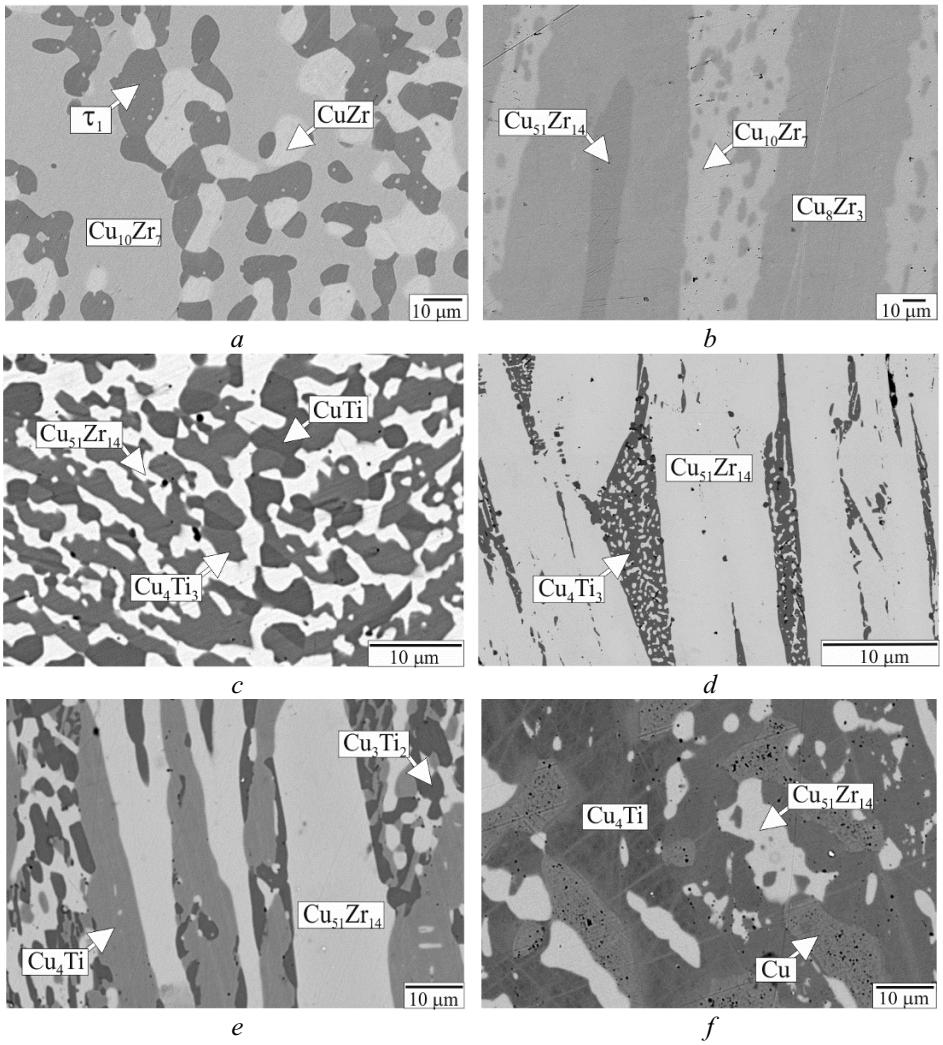

Fig. 5. Microstructure of alloys in the Cu–Ti–Zr system (in backscattered electrons) from the two-phase region—alloy 42 (*d*) and three-phase regions—alloys 30 (*a*); 39 (*b*); 38 (*c*); 43 (*e*); 47(*f*)

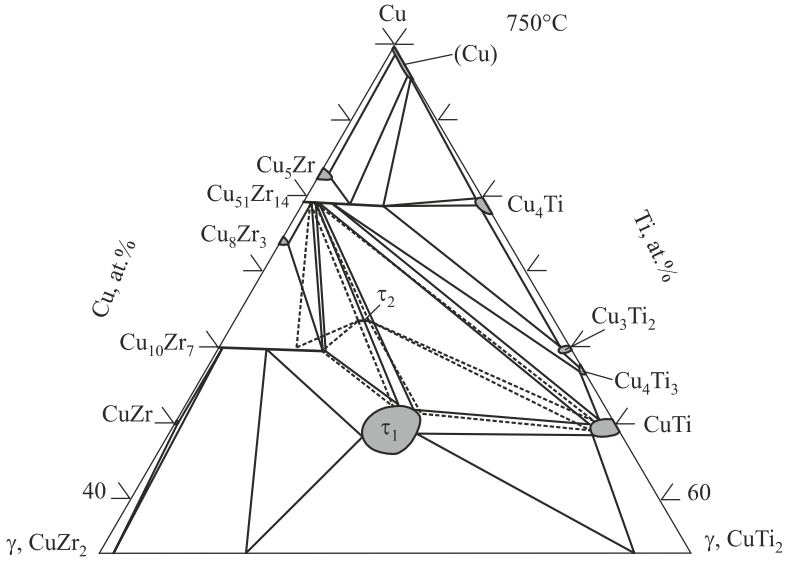

Fig. 6. Isothermal section of the Cu–Ti–Zr phase diagram in the $CuZr_2$–Cu–$CuTi_2$ region at 750°C [6]; our data are dashed

At 750°C, the τ_2 phase forms a number of two-phase equilibria—$\tau_2 + \tau_1$ (Figs. 2*b* and 4*a*), $\tau_2 + (Cu_{10}Zr_7)$, $\tau_2 + (Cu_{51}Zr_{14})$, and $\tau_2 + (CuTi)$ (Fig. 4*b*)—and three-phase equilibria—$\tau_2 + \tau_1 + (CuTi)$ (Fig. 2*c*, *d*), $\tau_2 + \tau_1 + (Cu_{10}Zr_7)$ (Fig. 2*e*), and $\tau_2 + (CuTi) + (Cu_{51}Zr_{14})$ (Fig. 2*f*). Three-phase alloys $\tau_2 + (Cu_{51}Zr_{14}) + (Cu_{10}Zr_7)$ were not obtained. Nevertheless, the three-phase $\tau_2 + (Cu_{51}Zr_{14}) + (Cu_{10}Zr_7)$ equilibrium in the isothermal section is clearly evidenced by the existence of boundary two-phase regions, such as $(Cu_{51}Zr_{14}) + (Cu_{10}Zr_7)$, $\tau_2 + (Cu_{51}Zr_{14})$, and $\tau_2 + (Cu_{10}Zr_7)$, established experimentally (Fig. 1).

The existence of phase equilibria involving the τ_2 phase and three-phase equilibria, such as $\tau_1 + (CuZr) + (Cu_{10}Zr_7)$ (Fig. 5*a*; Table 3) and $\tau_1 + (CuZr) + \gamma$ [1], significantly distinguishes our isothermal section at 750°C from the isothermal section at the same temperature provided in [6] Fig. 6. The existence of ternary $\tau_1 + (CuZr) + (Cu_{10}Zr_7)$ and $\tau_1 + (CuZr) + \gamma$ equilibria is consistent with the data at 703°C [5] and 800°C [7, 8].

Figure 1 shows that the $Cu_{51}Zr_{14}$-based phase dominates in the region under study. It participates in all expected three-phase equilibria: $(Cu_{51}Zr_{14}) + (Cu_{10}Zr_7) + (Cu_8Zr_3)$ (Fig. 5*b*), $(Cu_{51}Zr_{14}) + (Cu_4Ti_3) + (CuTi)$ (Fig. 5*c*), $(Cu_{51}Zr_{14}) + (Cu_4Ti) + (Cu_3Ti_2)$ (Fig. 5*e*), $(Cu_{51}Zr14) + (Cu_3Ti_2) + (Cu_4Ti_3)$, $(Cu_{51}Zr_{14}) + (Cu_4Ti) + (Cu)$ (Fig. 5*f*), and $(Cu_{51}Zr_{14}) + (Cu_5Zr) + (Cu)$. This agrees with the previous studies [6, 7].

Note that the paper [8] does not consider two three-phase equilibria: $(Cu_{51}Zr_{14}) + (Cu_{10}Zr_7) + (Cu_8Zr_3)$ and $(Cu_{51}Zr_{14}) + (Cu_5Zr) + (Cu)$.

The maximum titanium content of the $(Cu_{51}Zr_{14})$ phase reaches 10 at.%. Significant titanium solubility is also observed in the $(Cu_{10}Zr_7)$ phase, 12 at.%, and (CuZr) phase, 7.3 at.%, which is not the case for the Cu_5Zr and Cu_8Zr_3 phases (Fig. 1). The solubility of zirconium in binary compounds in the Cu–Ti system is insignificant: it is the highest in (CuTi), about 3 at.%. Data on the solubility of the third component agree well with the results reported in [6–8]. The only exception is [6], according to which titanium is hardly dissolved by CuZr.

CONCLUSIONS

In the ternary Cu–Ti–Zr system, a new ternary phase of hexagonal syngony has been found at 750°C and denoted by τ_2; its crystal structure has not been ascertained. This phase coexists in two-phase and three-phase equilibria with the Cu_2TiZr (τ_1), CuTi, $Cu_{10}Zr_7$, and $Cu_{51}Zr_{14}$ phases. The microhardness of the τ_2 phase is 6.0 ± ± 0.1 GPa.

There are 11 tie-line triangles in the isothermal section at 750°C in the CuZr–Cu–CuTi region. The $Cu_{51}Zr_{14}$ phase is in equilibria with most phases of the ternary system at 750°C. Its dominant role in the region reflects relatively high thermodynamic stability, which is consistent with its congruent formation in the binary Cu–Zr system.

ACKNOWLEDGEMENTS

The authors are grateful to L. A. Duma (Frantsevich Institute for Problems of Materials Science, National Academy of Sciences of Ukraine) and V. B. Sobolev (Technical Center under National Academy of Sciences of Ukraine) for technical support in the experiments.

REFERENCES

1. A. M. Storchak-Fedyuk, L. V. Artyukh, L. A. Duma, et al., “Phase equilibria in the Cu–Ti–Zr system at 750°C. I. The isothermal section with copper content from 0 to 50 at.%,” *Powder Metall. Met. Ceram.*, **56**, No. 1–2, 78–87 (2017).
2. E. Ence and H. A. Margolin, “A study of the Ti–Cu–Zr system and the structure of Ti_2Cu,” *Trans. Metal. Soc. AIME*, **221**, 320–322 (1961).
3. V. N. Chebotnikov and V. V. Molokanov, “Structure and properties of Ti_2Cu–Zr_2Cu alloys in the Ti–Zr–Cu system in amorphous and crystalline states,” *Izv. Akad. Nauk SSSR. Neorg. Mater.*, **26**, No. 5, 960–964 (1990).

4. Yu. K. Kovneristyi and A. G. Pashkovskaya, “Bulk amorphization of alloys in the intermetallic Ti–Cu–Zr system,” in: *Amorphous (Glassy) Metallic Materials* [in Russian], Inst. Metall. RAN, Moscow (1992), pp. 153–157.
5. C. G. Woychik and T. B. Massalski, “Phase diagram relationships in the system copper–titanium–zirconium,” *Z. Metallkd.*, **79**, No. 3, 149–153 (1988).
6. P. G. Qin, H. Wang, H. S. Zhang, et al., “The isothermal section of the Cu–Ti–Zr system at 1023 K measured with diffusion-triple approach,” *Mater. Sci. Eng. A*, **476**, 83–88 (2008).
7. U. E. Klotz, C. Liu, P. J. Uggowitzer, et al., “Experimental investigation of the Cu–Ti–Zr system at 800°C,” *Intermetallics*, **15**, 1666–1671 (2007).
8. W.-R. Chiang, K.-C. Hsieh, Y. A. Chang, et al., “Phase equilibrium in the Cu–Ti–Zr system at 800°C,” *Mater. Trans.*, **48**, No. 7, 1631–1634 (2007).
9. I. Ansara and V. Ivanchenko, “Cu–Ti (copper–titanium),” in: G. Effenberg (ed.), *MSIT Binary Evaluation Program*, MSIT Workplace, Materials, MSI (2002).
10. T. V. Massalski (ed.), P. R. Subramanian, H. Okomoto, et al., *Binary Alloy Phase Diagrams*, 2nd ed., 3 vols., ASM International, Materials Park, Ohio (1990), p. 3589.
11. T. Velikanova and M. Turchanin, “Copper–titanium–zirconium,” in: *Landolt-Börnstein: Numerical Data and Functional Relationships in Science and Technology*, W. Martiensen (ed.), New Series. Group IV: Physical Chemistry. Ternary Alloy Systems. Phase Diagrams, Crystallographic and Thermodynamic Data, Vol. 11C3, Springer-Verlag, Berlin, Heidelberg (2006), pp. 436–464.
12. M. Yu. Teslyuk, *Intermetallic Compounds with Laves Phase Structure* [in Russian], Nauka, Moscow (1969), p. 138.
13. X. Yan, X.-Q. Chen, A. Gritsiv, et al., “Crystal structure, phase stability, and elastic properties of the Laves phase $ZrTiCu_2$,” *Intermetallics*, **16**, 651–657 (2008).